
This project has received funding from the European Union's Horizon 2020 research and innovation programme under grant agreement No 101007417 having benefited from the access provided by IOM-CNR in Trieste (Italy) within the framework of the NFFA-Europe Pilot Transnational Access Activity, proposal ID101.

Investigating Structural, Optical, and Electron-Transport Properties of Lithium Intercalated Few-Layer MoS_2 Films: Unraveling the Influence of Disorder

J. Hrdá,[1] M. Moško,[1,2] I. Píš,[3] T. Vojteková,[1] L. Pribusová Slušná,[1] P. Hutár[1], M. Precner[1], E. Dobročka,[1] M. Španková,[1] M. Hulman[1], Š. Chromik,[1] P. Siffalovic,[4] F. Bondino[3] and M. Sojková[1*]*

[1] Institute of Electrical Engineering, SAS, Dúbravská cesta 9, 841 04 Bratislava, Slovakia

[2] Department of Experimental Physics, Faculty of Mathematics, Physics and Informatics, Comenius University in Bratislava, 842 48 Bratislava, Slovakia

[3] IOM-CNR, Istituto Officina dei Materiali, S.S. 14 km – 163.5, 34149 Basovizza, Trieste, Italy

[4] Institute of Physics, Slovak Academy of Sciences, Dúbravská cesta 9, 84511 Bratislava, Slovakia

Abstract:

Molybdenum disulfide is a promising candidate for various applications in electronics, optoelectronics, or alkali-ion batteries. The natural presence of the van der Waals gap allows intercalating alkali ions, such as lithium, into MoS_2 films. Intercalation can modify the electronic structure, as well as the electrical and optical properties. Here, we present a structural, optical, and electrical characterization of Li-intercalated few-layer MoS_2 films. The intercalation was carried out by annealing MoS_2 film in the presence of Li_2S powder, serving as a lithium source. The initial MoS_2 layers were prepared by pulsed laser deposition (PLD), and by sulfurization of 1 nm thick Mo film (TAC). The presence of lithium was confirmed by synchrotron-based X-ray Photoelectron Spectroscopy. The Raman spectroscopy, X-ray diffraction, and optical absorption measurements confirmed semiconducting behavior for all samples. All samples exhibited the thermally activated dependence of the electrical resistance, R, typical for the Efros-Shklovskii variable range hopping in a disordered semiconductor,

* **Author to whom correspondence should be addressed.**

Electronic mail: michaela.sojkova@savba.sk, jana.hrda@savba.sk

$\ln R(T) \propto (T_{ES}/T)^{1/2}$, where $k_B T_{ES}$ is the hopping activation energy. The PLD-grown MoS_2 samples exhibited a relatively mild initial disorder primarily caused by grain boundaries. Lithium intercalation led to an increase in disorder, evident in the increase of $k_B T_{ES}$ and a substantial rise in electrical resistance. The TAC-grown undoped MoS_2 sample already exhibited significant resistance, and the impact of Li intercalation on resistance was minimal. This observation was attributed to the fact that the TAC-grown MoS_2 samples exhibit a perturbed stoichiometry (the S:Mo ratio ~ 2.20), causing strong disorder even before Li intercalation. The electron doping caused by lithium, if any, was completely obscured by the effect of disorder.

Molybdenum disulfide (MoS_2) belongs to the layered two-dimensional transition metal dichalcogenides (TMDs) family. The structure of MoS_2 consists of the hexagonally arranged S-Mo-S atomic layers that have strong covalent bonds and individual layers are held together by the weak van der Waals forces. Among various TMDs, the MoS_2 is one of the most promising due to its abundant and non-toxic elements.[1,2] Moreover, MoS_2 is a semiconductor applicable in transistors,[3,4] solar cells,[5,6] photodetectors,[7,8] and sensors.[9–11] In addition, MoS_2 is useful in energy storage and conversion,[12–14] or as electrode material for lithium-ion[15,16] or sodium-ion[17] batteries.

Various modifications are applied to MoS_2 to tune its properties. These modifications include dimensional sizing,[18] strain engineering,[19,20] external field tunning,[21] doping,[22] and intercalation of guest species into the van der Waals gap.[23] Intercalation can modify the electronic structure, as well as the optical, and electrical properties, directly through electron doping or indirectly by inducing structure modification or disorder. Some alkali and alkaline earth metals with small ions radii occupy the space between MoS_2 layers rather than substitute the host atoms. These atoms are believed to transfer electrons to the MoS_2 layers, which is often associated with a phase transformation from semiconducting 2H structure to metallic 1T structure or disordered 1T (1T') phases.[24] Besides the phase transition, intercalation of guest species might lead to an exfoliation of bulk MoS_2.[25,26] Lithium intercalation/deintercalation of MoS_2 has been studied for a better understanding of charging-discharging cycles in Li-ion batteries.[27]

The properties of few-layer TMDs can also be affected by the fabrication method. For use in applications, uniform large-area few-layer MoS_2 films are essential, therefore, the growth techniques are more desirable than the exfoliation methods. Growth of a continuous-monolayer to few-layer MoS_2 films could be achieved using molecular beam epitaxy,[28] chemical vapor deposition,[29] thermally assisted conversion (TAC) - sulfurization of pre-deposited metal/metal

oxide layers,[30] or pulsed laser deposition (PLD).[31] Sulfurization of the pre-deposited Mo films is a practical method for the fabrication of large-area films of nanometer thickness. However, the nanocrystals are oriented rather randomly, with no long-range ordering within the layers. PLD is another suitable technique for the growth of highly crystalline MoS_2.[32] Španková et al. reported the growth of large-area few-monolayer thick MoS_2 films with excellent crystalline quality and thickness homogeneity on c-plane sapphire and GaN/sapphire substrates.[33]

In this work, we focused on electron transport measurements in as-grown and Li-doped MoS_2 films prepared by two different methods (PLD and sulfurization). The aim was to study the role of Li doping and disorder in the as-prepared films. The samples were characterized by structural, chemical composition, optical, and electrical measurements. The dominant types of disorder were identified in both undoped and Li-doped samples.

The initial MoS_2 layers were grown on the c-plane sapphire substrate by two different techniques: one-zone sulfurization of 1 nm Mo layer (denoted as TAC) and PLD using the MBE/PLD-2000 deposition system equipped with an excimer 248 nm laser Compex 102. For both, TAC and PLD-grown samples, lithium was incorporated into the as-prepared few-layer MoS_2 films by solid-state diffusion during the subsequent sulfurization process, where a part of sulfur powder was replaced by lithium sulfide (Li_2S) as a source of Li.[34] The powders of Li_2S and sulfur (with the Li_2S being 20% or 50% of the total weight) were placed in the middle of the one-zone furnace alongside the initial MoS_2 films and annealed at elevated temperatures for 30 minutes with the heating rate of 25 °C/min. The lithiation temperature was 800 °C and 600 °C for TAC and PLD-grown initial MoS_2 layers, respectively.

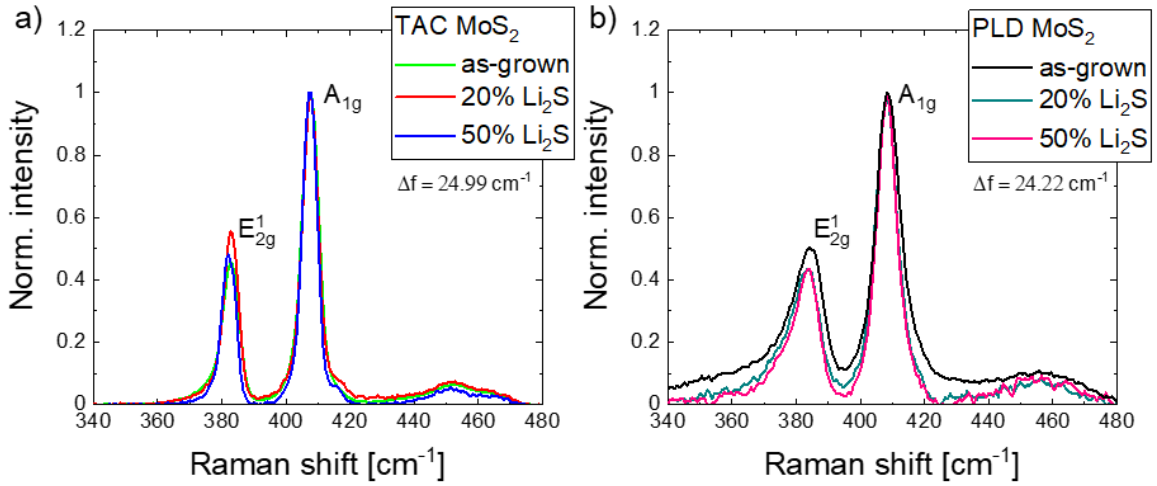

FIG. 1. Normalized Raman spectra of as-grown and Li-doped MoS_2 samples grown by TAC (a) and PLD (b)

A confocal Raman microscope (Alpha 300 R, WiTec, Germany) equipped with a laser excitation wavelength of 532 nm and a 50x objective was used to acquire Raman spectra. Fig. 1 shows the normalized Raman spectra of the undoped and Li-doped MoS_2 samples prepared by TAC and PLD. The existence of MoS_2 in all samples is validated by the presence of the characteristic in-plane E^1_{2g} (~ 383 cm^{-1}) and out-of-plane A_{1g} (~ 408 cm^{-1}) vibration modes. The frequency difference $\Delta f = (A_{1g}–E^1_{2g})$ is 24.99 cm^{-1} for the TAC-grown samples and 24.22 cm^{-1} for the PLD-grown samples. The peak positions and the frequency difference correspond to the bulk MoS_2. Counting the number of layers from the peak positions and the frequency difference is ambiguous,[35] so the thickness of the samples was estimated from x-ray reflectance measurements. The MoS_2 grown by sulfurization of 1 nm Mo film has a thickness of approximately 4 nm, corresponding to 5-6 monolayers (ML).[30] The thickness of the PLD-grown samples is about 5 ML. The positions of the main modes' peaks and frequency differences remain constant before and after Li-doping. Structural analysis of the as-prepared samples was done by x-ray diffraction (XRD) in a symmetrical θ/2θ configuration. The as-prepared and Li-doped MoS_2 films are c-plane oriented and exhibit epitaxial growth. Further details can be found in Figs. S1-S2 in the Supplementary material.

The chemical composition and stoichiometry of the MoS_2 layers were analyzed by means of synchrotron photoemission spectroscopy and x-ray photoemission spectroscopy (experimental details are provided in the Supplementary material). Li 1s spectra shown in Fig. 2 verify the lithiation of both TAC and PLD samples. The Li 1s spectra exhibit a dominant component centered at a binding energy of 55.8 ± 0.1 eV, attributed to Li atoms intercalated into MoS_2.[34] The minor Li 1s component at lower binding energies likely originates from the presence of Li hydroxide and oxide species.[36,37] The intensity ratio between Li 1s and Mo 4s peaks reflects the relative elemental atomic concentrations. The concentrations of Li measured in the studied samples are summarized in Table I. Similarly, the S:Mo stoichiometric ratio can be determined from S 2p and Mo 3d peak areas (Supplementary material Fig. S3).

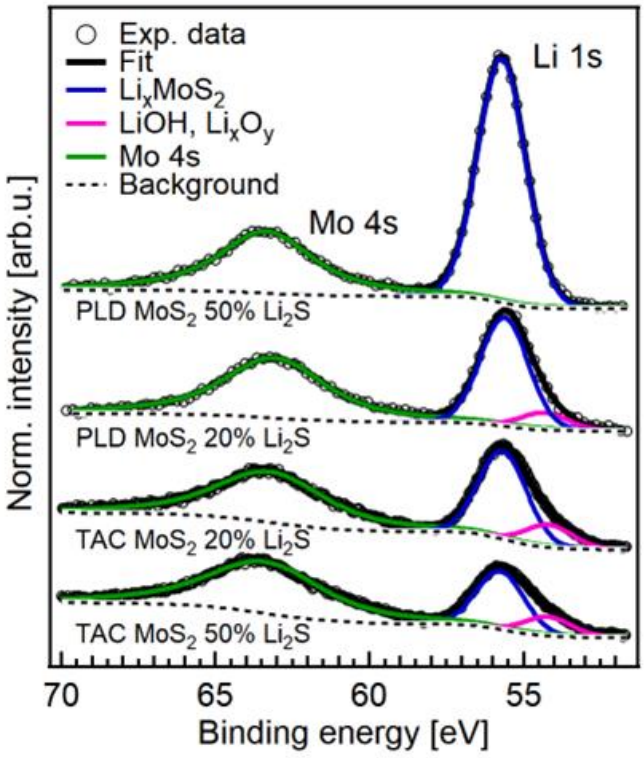

FIG. 2. Li 1s and Mo 4s photoelectron spectra for Li-doped TAC and PLD-grown MoS_2 films. The spectra were acquired at a photon energy of 120 eV.

Using the Shimadzu SolidSpec-3700 spectrophotometer in the UV–VIS range, we measured the transmittance and reflectance from the front side and back side of the samples. This approach provides the absorbance of the MoS_2 layers without assuming any particular

model of the layer dielectric function.[38] Fig. 3 shows the absorption spectra of the undoped and Li-doped samples prepared with 50% of Li_2S. All spectra are similar to those reported for the multi-layer samples with a similar number of MoS_2 monolayers,[39] all of them show the optical gap of 1.7 – 1.8 eV, demonstrating that both the undoped and Li-doped samples are semiconductors.

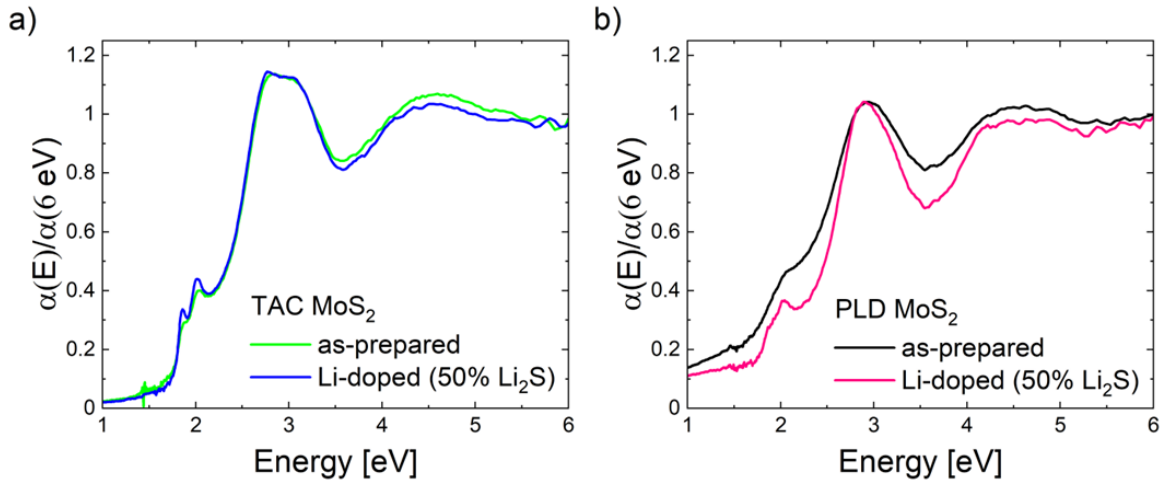

FIG. 3. Absorbance of as-prepared and Li-doped MoS_2 samples grown by a) TAC and b) PLD.

The sample resistance R as a function of temperature T was measured by the four-probe method using the Physical Property Measurement System – Model 6000, from Quantum Design Inc. Fig. 4a shows the measured R(T) data in terms of log R versus T. For all our samples the R(T) dependence tends to diverge with decreasing T, which is typical for the insulating transport regime.[40] The Li-free TAC-MoS_2 sample is much more resistive than the Li-free PLD-MoS_2 one. After introducing the Li atoms into the PLD-grown MoS_2 samples, their resistance dramatically increased with the increase of the Li concentration. In the TAC-grown samples, the effect of Li doping on the resistance magnitude is considerably weaker. We will now discuss these results in detail.

Fig. 4b shows the log R as a function of 1/T. Evidently, the data do not follow the Arrhenius dependence log R $\propto$ 1/T. Dependence log R $\propto$ 1/T is typical for the thermally activated transport in semiconductors and for the nearest neighbor hopping in disordered

solids,[40] as observed in previous transport studies of MoS_2.[41] However, in our case, the increase of log R with 1/T is slower than log R ∝ 1/T.

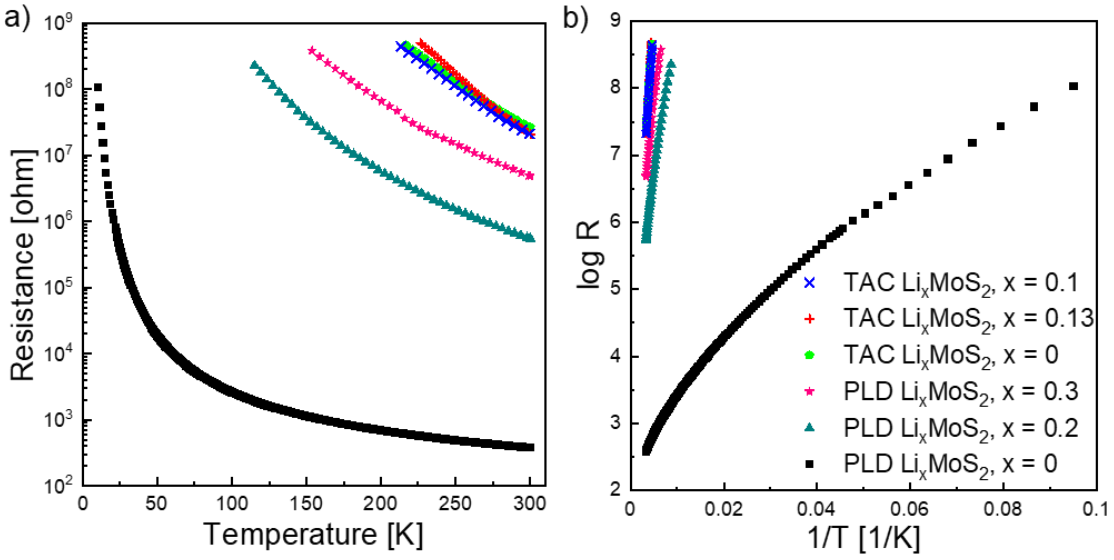

FIG. 4. Measured R (T) dependence for a series of the PLD-grown and TAC-grown MoS_2 layers with corresponding Li stochiometric coefficients. In panel (a) the data are shown as R versus T, in panel (b) as log R versus 1/T.

At low enough temperatures, transport in disordered solids occurs via the Mott variable range hopping (VRH) rather than via the nearest neighbor hopping.[40] For the Mott VRH, the electron localized at the Fermi level (E_F) moves to another localized state in an optimum hopping distance which is determined by the tradeoff between the lowest energy difference and the shortest hopping distance.[40] In a non-interacting disordered system, the density of states at the Fermi level, $N(E_F)$, is finite and the resistance of the two-dimensional disordered system is described by Mott VRH with R(T) dependence $\ln(R/R_{Mott}) = (T_{Mott}/T)^{1/3}$, where

$$k_B T_{Mott} = \frac{27}{\pi N(E_F) L_{loc}{}^2}, \quad (1)$$

is the hopping activation energy, with L_{loc} being the electron localization length and $1/(N(E_F)L_{loc}{}^2)$ being the electron energy spacing the electron overcomes in one hop.[40]

The Mott VRH dependence $\ln(R/R_{Mott}) = (T_{Mott}/T)^{1/3}$ has been observed at low temperatures in two-dimensional disordered MoS_2 flakes prepared by the exfoliation.[41,42] If the disordered film of interest is not sufficiently thin, the Mott VRH exhibits dependence $\ln(R/R_{Mott}) = (T_{Mott}/T)^{1/4}$, typical for three-dimensional systems.[40]

Another work reported that the exfoliated MoS_2 flakes treated in n-butyllithium exhibit the dependence $\ln(R/R_{ES}) = (T_{ES}/T)^{1/2}$,[43] typical for the Efros-Shklovskii VRH.[44] Efros and Shklovskii have shown that the Coulomb interaction between the localized electrons opens the Coulomb gap at the Fermi level which emerges in the vanishing of $N(E_F)$. As a result, below a certain critical temperature the Mott VRH dependence $\ln(R/R_{Mott}) = (T_{Mott}/T)^{1/3}$ changes to the Efros-Shklovskii VRH dependence $\ln(R/R_{ES}) = (T_{ES}/T)^{1/2}$ with activation energy[44]

$$k_B T_{ES} = \frac{\Gamma e^2}{4\pi\varepsilon_r\varepsilon_0 L_{loc}} \qquad (2)$$

where e is the electron charge, ε_0 is the permittivity of vacuum, ε_r is the relative permittivity of the system, and $\Gamma = 6.5$.[45] The Efros-Shklovskii dependence holds for any system dimensionality.

To determine which R(T) dependence supports our MoS_2 samples, the data from Fig. 4 were plotted in Fig. 5 as ln(R) versus $1/T^{1/2}$ and as ln(R) versus $1/T^{1/3}$. For better visibility, Fig. 5a displays solely the data for the Li-free PLD-grown MoS_2 sample, Fig. 5b shows the data for the Li-doped PLD-grown MoS_2 samples, and Fig. 5c shows the data for the TAC-grown MoS_2 samples, both as-grown and Li-doped. The solid lines represent linear fits to the data. The data in Fig. 5a support better the dependence $\ln R(T) \propto (T_{ES}/T)^{1/2}$, however, the data in Figs. 5b and 5c do not allows to distinguish between $\ln R(T) \propto (T_{ES}/T)^{1/2}$ and $\ln R(T) \propto (T_{Mott}/T)^{1/3}$, which is a frequently faced problem.[45]

To demonstrate that all our samples follow dependence ln R(T) $\propto (T_{ES}/T)^{1/2}$, we discuss the values of the fitting parameters T_{ES} and T_{Mott} which are presented in Tab. I along with the activation energies $k_B T_{ES}$ and $k_B T_{Mott}$. First, we examine the TAC samples and their T_{Mott} values. These values reach ~ 10^7 K, corresponding to activation energies $k_B T_{Mott}$ ~ 10^3 eV. For comparison, the largest reported value of T_{Mott} for MoS_2 films was about 10^5 K,[42] corresponding to the activation energy $k_B T_{Mott}$ ~ 10 eV. Generally, activation energies of various thermally activated transport processes in disordered solids rarely exceed 10 eV, in fact, they are usually much lower.[40] Thus, activation energies $k_B T_{Mott}$ ~ 10^3 eV are too large to be meaningful, which leads us to conclude that our TAC-grown MoS_2 samples do not exhibit the Mott VRH, despite the R(T) data in Fig. 5c follow the dependence $\ln(R/R_{Mott}) = (T_{Mott}/T)^{1/3}$ quite well. On the other hand, the values of T_{ES} are a hundred times lower and correspond to the activation energies $k_B T_{ES}$ ~ 7 – 12 eV, which are quantitatively reasonable. Hence, we conclude that the Li-free and Li-doped TAC-grown MoS_2 samples follow the Efros-Shklovskii VRH dependence $\ln(R/R_{ES}) = (T_{ES}/T)^{1/2}$. The same conclusion holds for the PLD-grown MoS_2 samples. In fact, for the Li-doped PLD-grown samples in Fig. 5b, energies $k_B T_{Mott}$ in Tab. I are still anomalously large (above 10^2 eV) while the energies $k_B T_{ES}$ are reasonable (less than 3.5 eV).

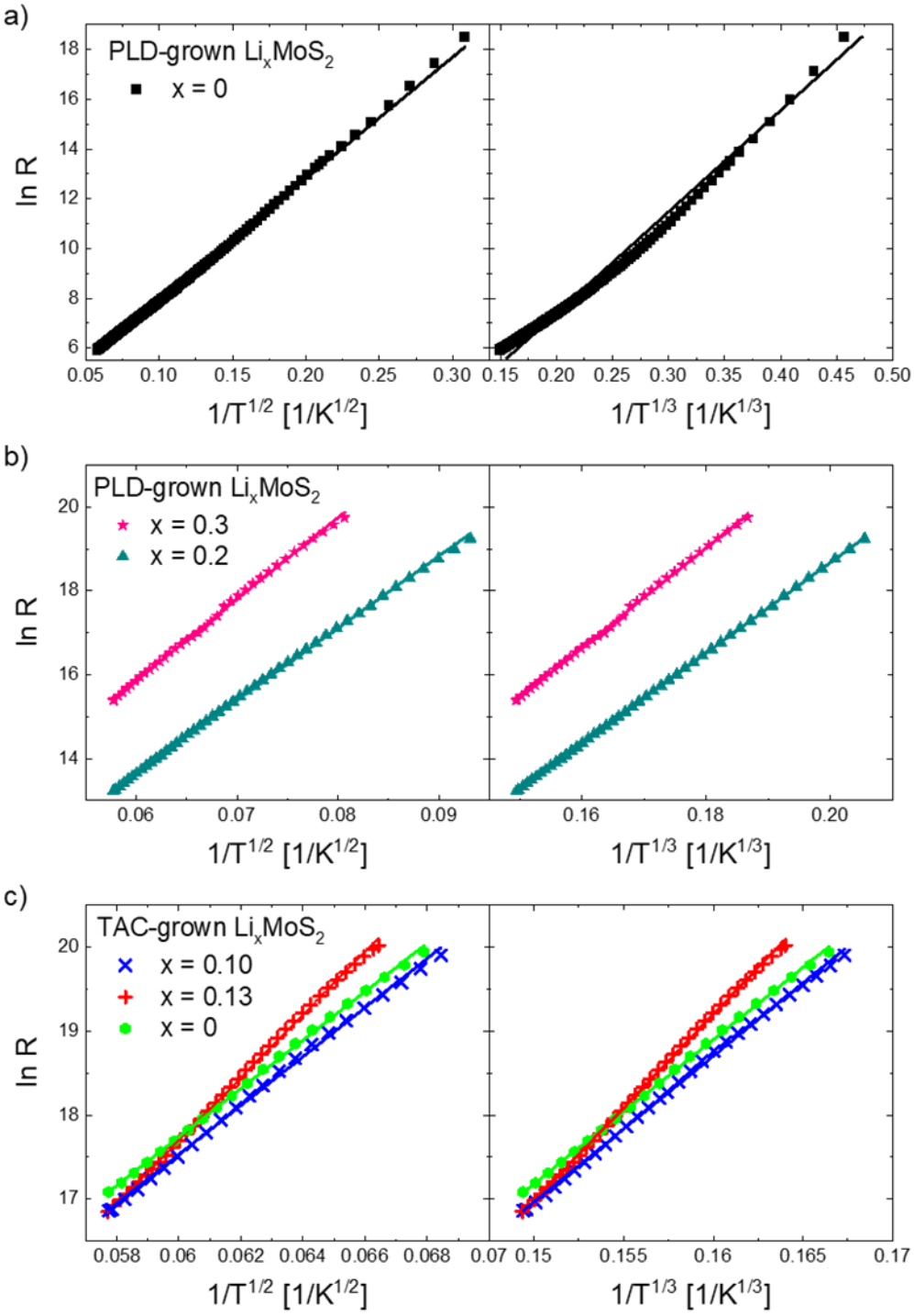

FIG. 5. Experimental data from Fig. 4 are plotted as ln R versus $1/T^{1/2}$ and as ln R versus $1/T^{1/3}$. (a) Data for the PLD-grown MoS_2 film without lithium, (b) data for the PLD-grown MoS_2 films with lithium stochiometric coefficients of $x = 0.2$ and $x = 0.3$, (c) data for the TAC-grown MoS_2 films without ($x = 0$) and with lithium doping ($x = 0.1$, $x = 0.13$). The solid lines show the fit of the experimental data by the dependencies $\ln(R/R_{ES}) = (T_{ES}/T)^{1/2}$ and $\ln(R/R_{Mott}) = (T_{Mott}/T)^{1/3}$. The values of the fitting parameters T_{ES} and T_{Mott} are shown in Tab. I.

To further support the above conclusions, using $k_B T_{Mott} \sim 10^3$ eV, we obtain from equation (1) the energy level spacing $1/(N(E_F)L_{loc}^2 \sim 10^2$ eV, which is again too large to be meaningful. On the other hand, if we use the activation energies $k_B T_{ES} \sim 0.22 - 12$ eV and

permittivity $\varepsilon_r \sim 5$ (valid for few-layer MoS_2 films[43,46]), from equation (2) we obtain the localization length $L_{loc} \sim 0.16 - 13$ nm. Here, even the smallest value, $L_{loc} \sim 0.16$ nm, is reasonably large and might correspond to a localized state at an impurity.

To distinguish between $\ln(R/R_{Mott}) = (T_{Mott}/T)^{1/3}$ and $\ln(R/R_{ES}) = (T_{ES}/T)^{1/2}$ directly, it would be advantageous to extend the R(T) measurements to significantly lower temperatures than those presented in Fig. 5. However, this would result in extremely high resistances that exceed our contemporary measurement capabilities.

Table I: Studied MoS_2 samples, amount of Li_2S/S, stochiometric coefficient of Li, and composition determined by photoemission spectroscopy, fitting temperatures T_{ES}, T_{Mott}, and corresponding activation energies k_BT_{ES}, k_BT_{Mott}, characterizing the transport mechanism in the samples.

Sample	Li_2S/S	Stoichiometric coefficient of Li - x	Composition Li_xMoS_y	T_{ES} [K]	k_BT_{ES} [eV]	T_{Mott} [K]	k_BT_{Mott} [eV]
TAC MoS_2	0%	0	$MoS_{2.2}$	82 942	7.1	5 049 152	435
TAC MoS_2	20%	x = 0.13 ± 0.03	$Li_{0.1}MoS_{2.2}$	84 772	7.3	5 240 436	451
TAC MoS_2	50%	x = 0.10 ± 0.02	$Li_{0.1}MoS_{2.2}$	140218	12.1	10 972 142	945
PLD MoS_2	0%	0	$MoS_{2.0}$	2 551	0.22	67 103	5.8
PLD MoS2	20%	x = 0.2 ± 0.1	$Li_{0.2}MoS_{2.1}$	29 503	2.54	1 252 645	108
PLD MoS2	50%	x = 0.3 ± 0.1	$Li_{0.3}MoS_{2.0}$	37 653	3.24	1 681 548	145

According to Tab. 1, k_BT_{ES} for the undoped ($x = 0$) TAC-grown MoS_2 sample is thirty times larger than k_BT_{ES} for the undoped PLD-grown MoS_2 sample. According to equation (2), the larger the activation energy k_BT_{ES} the smaller the localization length L_{loc} due to disorder. This means that disorder in the undoped TAC-grown sample is much stronger than in the undoped PLD-grown sample. The question is what causes this strong disorder. Our chemical composition analyses (Tab. 1 and Supplementary Tab. TS1) show that the TAC-grown MoS_2 samples are non-stoichiometric (the S:Mo ratio is about 2.2), while in the PLD-grown MoS_2 samples, the S:Mo ratio is close to 2. It is important to mention that excess sulfur does not affect the resulting XRD patterns demonstrating the crystalline arrangement (Supplementary Fig. S1). This suggests that the excess sulfur fills the gaps between the neighboring monolayers as an impurity disorder, causing the substantial electrical resistance of the TAC-grown samples.

What remains to be determined is the origin of the disorder in the undoped PLD grown MoS_2 sample. Using atomic force microscopy (see Supplementary Fig. S4-S5 and Tab. TS2), we estimated the lateral grain size distribution. The size of grains L_{grains} for MoS_2 layers grown by TAC and PLD are in the range of 3 – 30 nm suggesting negligible differences in grain sizes for these two fabrication methods. From equation (2) we find for the undoped PLD–grown sample the localization length $L_{loc} \sim 13$ nm. It clearly exceeds L_{grain}, suggesting that electron localization in the undoped PLD–grown sample is caused by disorder due to the grain boundaries. For the undoped TAC–grown sample is $L_{loc} \sim 0.3$ nm. It is evident that such a small L_{loc} cannot be ascribed to grain boundary disorder with $L_{grain} \sim 3$ - 30 nm, therefore it has to be attributed to the non-stoichiometry, as discussed above. The disorder induced by the minor traces of impurities detected via photoemission spectroscopy (see Supplementary Tab. TS1) is likely negligible.

Furthermore, the data in Tab. I reveal that Li intercalation introduces additional disorder, as the increase of x above zero is accompanied by the rise of $k_B T_{ES}$. The activation energy $k_B T_{ES}$ increases with the stoichiometric coefficient of Li, x, with one exception - the TAC-grown sample with $x = 0.1$ exhibits a larger $k_B T_{ES}$ than the sample with $x = 0.13$. This discrepancy could be attributed to experimental uncertainties in the Li concentration determination (in Tab. I), suggesting that the actual lithium concentration in the doped TAC sample synthesized using a 50% Li_2S powder composition might be slightly higher than in the one where 20% Li_2S powder was used, as would be expected.

In conclusion, Li-intercalated few-layer MoS_2 films were fabricated using an innovative approach, the one-zone sulfurization with Li_2S powder which serves as a source of lithium. The initial MoS_2 layers were grown by TAC and PLD. The Li intercalation did not affect the 2H hexagonal structure and semiconducting character of our MoS_2 layers, as verified by Raman, XRD, and optical measurements. Electrical R(T) measurements revealed that all

samples exhibited the insulating dependence $\ln(R/R_{ES}) = (T_{ES}/T)^{1/2}$, typical for the Efros-Shklovskii variable range hopping in a disordered semiconductor.[44] In recent works[47–49] the Efros-Shklovskii VRH was observed in undoped semiconducting MoS_2 films only at very low temperatures. On the other hand, in our work, Efros-Shklovskii VRH was observed in wide temperature range (from 300 K down to low temperatures). This was caused by higher disorder in our samples. The same $\ln(R/R_{ES}) = (T_{ES}/T)^{1/2}$ dependence was manifested by the disordered 1T/1T′ MoS_2 monolayer flakes which are however metallic.[43] The Li intercalation in our MoS_2 layers induced additional disorder, further enhancing the Efros-Shklovskii insulating regime of electronic transport already present in the samples. The strong disorder observed in the undoped TAC-MoS_2 samples is attributed to sulfur non-stoichiometry. The weak disorder in the undoped PLD-grown MoS_2 samples is due to the grain boundaries. Li intercalation might also induce electron doping; however, this effect was entirely obscured by the dominant effect of disorder, which significantly amplifies resistance.

Supplementary material

See supplementary material for supporting results, including XRD, Photoelectron Spectroscopy Analysis, AFM images and grain size distribution for all undoped and Li-doped MoS_2 layers.

Acknowledgments

The research leading to this result has been supported by the project CALIPSOplus under Grant Agreement 730872 from the EU Framework Programme for Research and Innovation HORIZON 2020. This project has received funding from the European Union's Horizon 2020 research and innovation programme under grant agreement No 101007417 having benefited from the access provided by IOM-CNR in Trieste (Italy) within the framework of the NFFA-Europe Pilot Transnational Access Activity, proposal ID101. XPS measurements carried out at the BACH beamline of CNR at the Elettra synchrotron facility in Trieste were performed thanks to the mobility project CNR-SAV-20-03. This study was conducted during the implementation

of the project Building-up Centre for Advanced Materials Application of the Slovak Academy of Sciences, ITMS project code 313021 T081, supported by the Research & Innovation Operational Programme funded by the ERDF. The Slovak Research and Development Agency supported this work through projects: APVV-19-0365, APVV-21-0231, and the Slovak Grant Agency for Science's projects VEGA2/0068/21 and VEGA2/0140/22 also supported the research. We acknowledge Dr. Maroš Gregor for laboratory XPS measurements. I.P. and F.B. acknowledge funding from EUROFEL project (RoadMap Esfri).

DATA AVAILABILITY

The data that support the findings of this study are available from the corresponding author upon reasonable request. The synchrotron photoemission spectroscopy data are openly available in the Zenodo repository at https://doi.org/10.5281/zenodo.10389596.

Declaration of Competing Interest

The authors have no conflicts to disclose.

REFERENCES:

[1] A.K. Singh, P. Kumar, D.J. Late, A. Kumar, S. Patel, and J. Singh, "2D layered transition metal dichalcogenides (MoS2): Synthesis, applications and theoretical aspects," Applied Materials Today **13**, 242–270 (2018).

[2] D. Gupta, V. Chauhan, and R. Kumar, "A comprehensive review on synthesis and applications of molybdenum disulfide (MoS2) material: Past and recent developments," Inorganic Chemistry Communications **121**, 108200 (2020).

[3] F. Wu, H. Tian, Y. Shen, Z. Hou, J. Ren, G. Gou, Y. Sun, Y. Yang, and T.-L. Ren, "Vertical MoS2 transistors with sub-1-nm gate lengths," Nature **603**(7900), 259–264 (2022).

[4] J. Lin, B. Wang, Z. Yang, G. Li, X. Zou, Y. Chai, X. Liu, and L. Liao, "High-current MoS2 transistors with non-planar gate configuration," Science Bulletin **66**(8), 777–782 (2021).

[5] M.-L. Tsai, S.-H. Su, J.-K. Chang, D.-S. Tsai, C.-H. Chen, C.-I. Wu, L.-J. Li, L.-J. Chen, and J.-H. He, "Monolayer MoS_2 Heterojunction Solar Cells," ACS Nano **8**(8), 8317–8322 (2014).

[6] R. Singh, A. Giri, M. Pal, K. Thiyagarajan, J. Kwak, J.-J. Lee, U. Jeong, and K. Cho, "Perovskite solar cells with an MoS_2 electron transport layer," J. Mater. Chem. A **7**(12), 7151–7158 (2019).

[7] Y. Xie, B. Zhang, S. Wang, D. Wang, A. Wang, Z. Wang, H. Yu, H. Zhang, Y. Chen, M. Zhao, B. Huang, L. Mei, and J. Wang, "Ultrabroadband MoS_2 Photodetector with Spectral Response from 445 to 2717 nm," Adv. Mater. **29**(17), 1605972 (2017).

[8] N. Wazir, R. Liu, C. Ding, X. Wang, X. Ye, X. Lingling, T. Lu, L. Wei, and B. Zou, "Vertically Stacked $MoSe_2$ /MoO_2 Nanolayered Photodetectors with Tunable Photoresponses," ACS Appl. Nano Mater. **3**(8), 7543–7553 (2020).

[9] Y. Han, D. Huang, Y. Ma, G. He, J. Hu, J. Zhang, N. Hu, Y. Su, Z. Zhou, Y. Zhang, and Z. Yang, "Design of Hetero-Nanostructures on MoS_2 Nanosheets To Boost NO_2 Room-Temperature Sensing," ACS Appl. Mater. Interfaces **10**(26), 22640–22649 (2018).

[10] N.-F. Chiu, and T.-L. Lin, "Affinity capture surface carboxyl-functionalized MoS2 sheets to enhance the sensitivity of surface plasmon resonance immunosensors," Talanta **185**, 174–181 (2018).

[11] T. De Silva, M. Fawzy, A. Hasani, H. Ghanbari, A. Abnavi, A. Askar, Y. Ling, M.R. Mohammadzadeh, F. Kabir, R. Ahmadi, M. Rosin, K.L. Kavanagh, and M.M. Adachi, "Ultrasensitive rapid cytokine sensors based on asymmetric geometry two-dimensional MoS2 diodes," Nat Commun **13**(1), 7593 (2022).

[12] Y. Li, H. Wang, L. Xie, Y. Liang, G. Hong, and H. Dai, "MoS_2 Nanoparticles Grown on Graphene: An Advanced Catalyst for the Hydrogen Evolution Reaction," J. Am. Chem. Soc. **133**(19), 7296–7299 (2011).

[13] N. Islam, S. Wang, J. Warzywoda, and Z. Fan, "Fast supercapacitors based on vertically oriented MoS2 nanosheets on plasma pyrolyzed cellulose filter paper," Journal of Power Sources **400**, 277–283 (2018).

[14] J. Gao, Y.D. Kim, L. Liang, J.C. Idrobo, P. Chow, J. Tan, B. Li, L. Li, B.G. Sumpter, T. Lu, V. Meunier, J. Hone, and N. Koratkar, "Transition-Metal Substitution Doping in Synthetic Atomically Thin Semiconductors," Adv. Mater. **28**(44), 9735–9743 (2016).

[15] C. Feng, J. Ma, H. Li, R. Zeng, Z. Guo, and H. Liu, "Synthesis of molybdenum disulfide (MoS2) for lithium ion battery applications," Materials Research Bulletin **44**(9), 1811–1815 (2009).

[16] H. Hwang, H. Kim, and J. Cho, "MoS_2 Nanoplates Consisting of Disordered Graphene-like Layers for High Rate Lithium Battery Anode Materials," Nano Lett. **11**(11), 4826–4830 (2011).

[17] X. Geng, Y. Jiao, Y. Han, A. Mukhopadhyay, L. Yang, and H. Zhu, "Freestanding Metallic 1T MoS_2 with Dual Ion Diffusion Paths as High Rate Anode for Sodium-Ion Batteries," Adv. Funct. Mater. **27**(40), 1702998 (2017).

[18] X. Zhang, Z. Lai, Z. Liu, C. Tan, Y. Huang, B. Li, M. Zhao, L. Xie, W. Huang, and H. Zhang, "A facile and universal top-down method for preparation of monodisperse transition-metal dichalcogenide nanodots.," Angew Chem Int Ed Engl **54**(18), 5425–5428 (2015).

[19] T. Peña, S.A. Chowdhury, A. Azizimanesh, A. Sewaket, H. Askari, and S.M. Wu, "Strain engineering 2D MoS $_2$ with thin film stress capping layers," 2D Mater. **8**(4), 045001 (2021).

[20] L. Kou, A. Du, C. Chen, and T. Frauenheim, "Strain engineering of selective chemical adsorption on monolayer MoS $_2$," Nanoscale **6**(10), 5156–5161 (2014).

[21] E.J.G. Santos, and E. Kaxiras, "Electrically Driven Tuning of the Dielectric Constant in MoS $_2$ Layers," ACS Nano **7**(12), 10741–10746 (2013).

[22] M.D. Sharma, C. Mahala, B. Modak, S. Pande, and M. Basu, "Doping of MoS $_2$ by 'Cu' and 'V': An Efficient Strategy for the Enhancement of Hydrogen Evolution Activity," Langmuir **37**(16), 4847–4858 (2021).

[23] F. Xiong, H. Wang, X. Liu, J. Sun, M. Brongersma, E. Pop, and Y. Cui, "Li Intercalation in MoS $_2$: In Situ Observation of Its Dynamics and Tuning Optical and Electrical Properties," Nano Lett. **15**(10), 6777–6784 (2015).

[24] G. Zhu, J. Liu, Q. Zheng, R. Zhang, D. Li, D. Banerjee, and D.G. Cahill, "Tuning thermal conductivity in molybdenum disulfide by electrochemical intercalation," Nat Commun **7**(1), 13211 (2016).

[25] X. Fan, P. Xu, D. Zhou, Y. Sun, Y.C. Li, M.A.T. Nguyen, M. Terrones, and T.E. Mallouk, "Fast and Efficient Preparation of Exfoliated 2H MoS $_2$ Nanosheets by Sonication-Assisted Lithium Intercalation and Infrared Laser-Induced 1T to 2H Phase Reversion," Nano Lett. **15**(9), 5956–5960 (2015).

[26] J. Peng, J. Wu, X. Li, Y. Zhou, Z. Yu, Y. Guo, J. Wu, Y. Lin, Z. Li, X. Wu, C. Wu, and Y. Xie, "Very Large-Sized Transition Metal Dichalcogenides Monolayers from Fast Exfoliation by Manual Shaking," J. Am. Chem. Soc. **139**(26), 9019–9025 (2017).

[27] M. Azhagurajan, T. Kajita, T. Itoh, Y.-G. Kim, and K. Itaya, "In Situ Visualization of Lithium Ion Intercalation into MoS $_2$ Single Crystals using Differential Optical Microscopy with Atomic Layer Resolution," J. Am. Chem. Soc. **138**(10), 3355–3361 (2016).

[28] D. Fu, X. Zhao, Y.-Y. Zhang, L. Li, H. Xu, A.-R. Jang, S.I. Yoon, P. Song, S.M. Poh, T. Ren, Z. Ding, W. Fu, T.J. Shin, H.S. Shin, S.T. Pantelides, W. Zhou, and K.P. Loh, "Molecular Beam Epitaxy of Highly Crystalline Monolayer Molybdenum Disulfide on Hexagonal Boron Nitride," J. Am. Chem. Soc. **139**(27), 9392–9400 (2017).

[29] Y.-H. Lee, X.-Q. Zhang, W. Zhang, M.-T. Chang, C.-T. Lin, K.-D. Chang, Y.-C. Yu, J.T.-W. Wang, C.-S. Chang, L.-J. Li, and T.-W. Lin, "Synthesis of Large-Area MoS $_2$ Atomic Layers with Chemical Vapor Deposition," Adv. Mater. **24**(17), 2320–2325 (2012).

[30] M. Sojková, K. Vegso, N. Mrkyvkova, J. Hagara, P. Hutár, A. Rosová, M. Čaplovičová, U. Ludacka, V. Skákalová, E. Majková, P. Siffalovic, and M. Hulman, "Tuning the orientation of few-layer MoS2 films using one-zone sulfurization," RSC Adv. **9**(51), 29645–29651 (2019).

[31] Y.-T. Ho, C.-H. Ma, T.-T. Luong, L.-L. Wei, T.-C. Yen, W.-T. Hsu, W.-H. Chang, Y.-C. Chu, Y.-Y. Tu, K.P. Pande, and E.Y. Chang, "Layered MoS $_2$ grown on *c* -sapphire by pulsed laser deposition: Layered MoS_2 grown on *c* -sapphire by pulsed laser deposition," Phys. Status Solidi RRL **9**(3), 187–191 (2015).

[32] C.R. Serrao, A.M. Diamond, S.-L. Hsu, L. You, S. Gadgil, J. Clarkson, C. Carraro, R. Maboudian, C. Hu, and S. Salahuddin, "Highly crystalline MoS $_2$ thin films grown by pulsed laser deposition," Appl. Phys. Lett. **106**(5), 052101 (2015).

[33] M. Španková, Š. Chromik, E. Dobročka, L. Pribusová Slušná, M. Talacko, M. Gregor, B. Pécz, A. Koos, G. Greco, S.E. Panasci, P. Fiorenza, F. Roccaforte, Y. Cordier, E. Frayssinet, and F. Giannazzo, "Large-Area MoS2 Films Grown on Sapphire and GaN Substrates by Pulsed Laser Deposition," Nanomaterials **13**(21), 2837 (2023).

[34] M. Sojková, I. Píš, J. Hrdá, T. Vojteková, L. Pribusová Slušná, K. Vegso, P. Siffalovic, P. Nadazdy, E. Dobročka, M. Krbal, P.J. Fons, F. Munnik, E. Magnano, M. Hulman, and F. Bondino, "Lithium-Induced Reorientation of Few-Layer MoS $_2$ Films," Chem. Mater. **35**(16), 6246–6257 (2023).

[35] H. Li, Q. Zhang, C.C.R. Yap, B.K. Tay, T.H.T. Edwin, A. Olivier, and D. Baillargeat, "From Bulk to Monolayer MoS2: Evolution of Raman Scattering," Adv. Funct. Mater. **22**(7), 1385–1390 (2012).

[36] D. Aurbach, I. Weissman, A. Schechter, and H. Cohen, "X-ray Photoelectron Spectroscopy Studies of Lithium Surfaces Prepared in Several Important Electrolyte Solutions. A Comparison with Previous Studies by Fourier Transform Infrared Spectroscopy," Langmuir **12**(16), 3991–4007 (1996).

[37] D. Aurbach, E. Pollak, R. Elazari, G. Salitra, C.S. Kelley, and J. Affinito, "On the Surface Chemical Aspects of Very High Energy Density, Rechargeable Li–Sulfur Batteries," J. Electrochem. Soc. **156**(8), A694 (2009).

[38] L. Pribusová Slušná, T. Vojteková, J. Hrdá, H. Pálková, P. Siffalovic, M. Sojková, K. Végsö, P. Hutár, E. Dobročka, M. Varga, and M. Hulman, "Optical Characterization of Few-Layer PtSe $_2$ Nanosheet Films," ACS Omega **6**(51), 35398–35403 (2021).

[39] M. Ye, D. Winslow, D. Zhang, R. Pandey, and Y. Yap, "Recent Advancement on the Optical Properties of Two-Dimensional Molybdenum Disulfide (MoS2) Thin Films," Photonics **2**(1), 288–307 (2015).

[40] N.F. Mott, and E.A. Davis, *Electronic Processes in Non-Crystalline Materials*, 2nd ed (Clarendon Press, Oxford, 2012).

[41] H. Qiu, T. Xu, Z. Wang, W. Ren, H. Nan, Z. Ni, Q. Chen, S. Yuan, F. Miao, F. Song, G. Long, Y. Shi, L. Sun, J. Wang, and X. Wang, "Hopping transport through defect-induced localized states in molybdenum disulphide," Nat Commun **4**(1), 2642 (2013).

[42] J. Xue, S. Huang, J.-Y. Wang, and H.Q. Xu, "Mott variable-range hopping transport in a MoS $_2$ nanoflake," RSC Adv. **9**(31), 17885–17890 (2019).

[43] N. Papadopoulos, G.A. Steele, and H.S.J. Van Der Zant, "Efros-Shklovskii variable range hopping and nonlinear transport in 1 T / 1 T ′ − MoS 2," Phys. Rev. B **96**(23), 235436 (2017).

[44] B.I. Shklovskiĭ, A.L. Efros, and S. Luryi, *Electronic Properties of Doped Semiconductors* (Springer-Verlag, Berlin Heidelberg New York [Etc.], 1984).

[45] D.N. Tsigankov, and A.L. Efros, "Variable Range Hopping in Two-Dimensional Systems of Interacting Electrons," Phys. Rev. Lett. **88**(17), 176602 (2002).

[46] D. Davelou, G. Kopidakis, G. Kioseoglou, and I.N. Remediakis, “MoS2 nanostructures: Semiconductors with metallic edges,” Solid State Communications **192**, 42–46 (2014).

[47] M. Masseroni, T. Qu, T. Taniguchi, K. Watanabe, T. Ihn, and K. Ensslin, “Evidence of the Coulomb gap in the density of states of MoS_2,” Phys. Rev. Research **5**(1), 013113 (2023).

[48] J. Cheng, S. Poehler, M. Laskar, L. Ma, S. Kannappan, S. Rajan, Y. Wu, and W. Lu, “Temperature dependent carrier transport in few-layered MoS_2 : from hopping to band transport,” J. Phys. D: Appl. Phys. **55**(19), 195109 (2022).

[49] I. Castillo, T. Sohier, M. Paillet, D. Cakiroglu, C. Consejo, C. Wen, F. Wasem Klein, M.-Q. Zhao, A. Ouerghi, S. Contreras, A.T.C. Johnson, M.J. Verstraete, B. Jouault, and S. Nanot, “Metal-insulator crossover in monolayer MoS_2,” Nanotechnology **34**(33), 335202 (2023).

Supplementary Material for:

Investigating Structural, Optical, and Electron-Transport Properties of Lithium Intercalated Few-Layer MoS_2 Films: Unraveling the Influence of Disorder

J. Hrdá,[1] M. Moško,[1,2] I. Píš,[3] T. Vojteková,[1] L. Pribusová Slušná,[1] P. Hutár[1], M. Precner[1], E. Dobročka,[1] M. Španková,[1] M. Hulman[1], Š. Chromik,[1] P. Siffalovic,[4] F. Bondino[3] and M. Sojková[1]

[1] Institute of Electrical Engineering, SAS, Dúbravská cesta 9, 841 04 Bratislava, Slovakia

[2] Department of Experimental Physics, Faculty of Mathematics, Physics and Informatics, Comenius University in Bratislava, 842 48 Bratislava, Slovakia

[3] IOM-CNR, Istituto Officina dei Materiali, S.S. 14 km – 163.5, 34149 Basovizza, Trieste, Italy

[4] Institute of Physics, Slovak Academy of Sciences, Dúbravská cesta 9, 84511 Bratislava, Slovakia

XRD Analysis - Supplementary Fig. S1 - S2

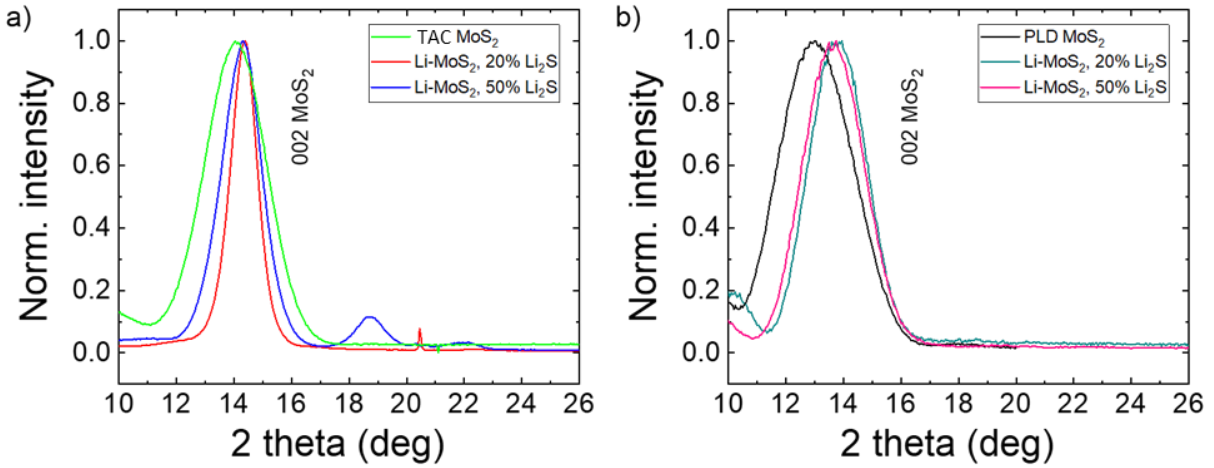

FIG. S1. – XRD patterns of the as-grown and Li-doped MoS_2 were obtained with a diffractometer Bruker D8 DISCOVER equipped with a rotating anode (Cu Kα) working at the power of 12 kW. (a) The initial MoS_2 layer (green) was grown by the one-zone sulfurization from 1 nm thick Mo film. The 002 diffraction was at 2 theta 14.05°, after Li doping (red and blue) the 2 theta of the main diffraction peak shifted slightly to 14.40°. This shift might be assigned to the change in lattice parameters of MoS_2 after intercalation with Li,[1] combined with the reduction of the in-plane strains present in the undoped MoS_2 sample.[2] (b) PLD-grown MoS_2 before (black) and after Li-doping (cyan and pink). The 002 of original MoS_2 was at 2 theta equals 13°, after Li-doping it rises to 13.75°. The same arguments as for the TAC-grown samples might be applied to explain this shift.

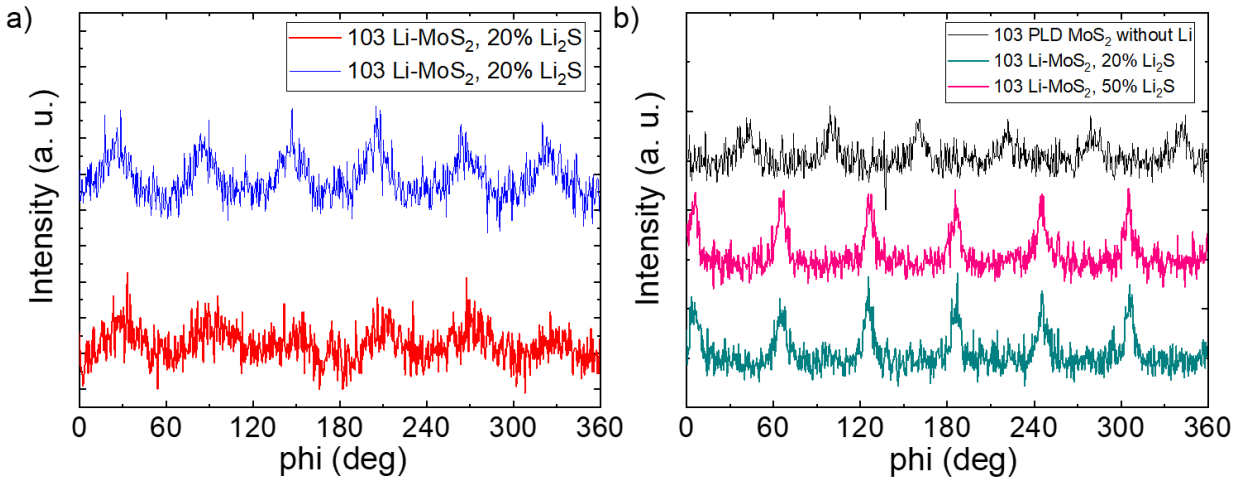

FIG. S2. – The in-plane ordering of the Li-doped (a) TAC-grown, and (b) PLD-grown MoS_2 layers was determined from azimuthal φ-scans. We have chosen the strongest 103 diffraction of the hexagonal MoS_2 phase for analysis. Epitaxial ordering was observed for all Li-doped MoS_2. Six peaks separated by 60° are present in the spectra, which corresponds to the hexagonal symmetry of 2H-MoS_2. The presence of distinct maxima in φ-scans indicates a tendency of the layers to grow epitaxially. The initial MoS_2 layer grown by TAC was originally not ordered in the a-b plane.

Photoelectron Spectroscopy Analysis - Supplementary FIG. S3, Tab. TS1

The chemical composition of Li-doped MoS_2 thin films was investigated using high-resolution synchrotron photoemission spectroscopy carried out at the BACH beamline of CNR at the Elettra synchrotron facility (in Trieste, Italy). Photoemission spectra were acquired using a Scienta R3000 hemispherical analyzer positioned at an angle of 60° relative to the X-ray incidence direction. The X-rays were linearly polarized with the polarization vector parallel to the scattering plane. The spectra were recorded in normal emission geometry at a take-off angle of 90° using photon energies of 605, 270, and 120 eV and a total instrumental resolution of 0.2 eV. To reduce the surface charging, the samples' temperatures were maintained at 150°C during data acquisition. Binding energies were referenced to the S $2p_{3/2}$ peak of thin MoS_2 films (161.95 ± 0.05 eV).[3–6] The core-level spectra were fitted with Voigt functions, except for Mo 3d where Gaussian-Lorentzian product functions provided better results. Shirley-type background was applied when appropriate; otherwise, a linear background was subtracted.

Elemental atomic concentrations were determined from the peak areas of the respective elements and the corresponding sensitivity factors. All intensities were normalized to the incident X-ray flux. The relative sensitivity factor for Mo 3d and S 2p core levels was determined from spectra obtained from a reference MoS_2 sample (MoS_2 powder from Acros Organics, 98.5%.). Relative sensitivity factors S_i^j for other elements (i) and core levels (j) were estimated using theoretical parameters:

$$S_i^j = T\lambda_i^j \sigma_i^j (1+0.625\beta_i^j),$$

where T is the analyzer transmission function,[7] λ_i^j is the inelastic mean free path of analyzed photoelectrons in MoS_2,[8] σ_i^j and β_i^j are theoretical photoionization cross-section and related asymmetry parameters, respectively.[9]

Lithium concentrations were determined by the integrated intensity ratios of Li 1s and Mo 4s peaks. Contribution from lithium oxides and hydroxides was subtracted. Both Li 1s and Mo 4s spectra were recorded at three different photon energies (120, 270, and 605 eV) and the obtained Li:Mo concentration ratio values were averaged.

The relative concentrations of Te and Na impurities were estimated from the peak areas of Te 4d, Na 2p, and Mo 4p measured at a photon energy of 120 eV, while the concentration of potassium was determined from the relative intensities of K 2p and Mo 3d peaks acquired at a photon energy of 605 eV.

Signals from aluminum and oxygen were excluded from the quantitative analysis due to the strong contribution from the sapphire wafer substrate. Additionally, only negligible amounts of Mo oxides were detected in the Mo 3d spectra.

The chemical composition of undoped PLD MoS_2 was analyzed by laboratory XPS setup (Omicron multiprobe system with the hemispherical analyzer, Scienta Omicron, Taunusstein, Germany), using monochromatic Al K-alpha X-rays - 1486.6 eV.

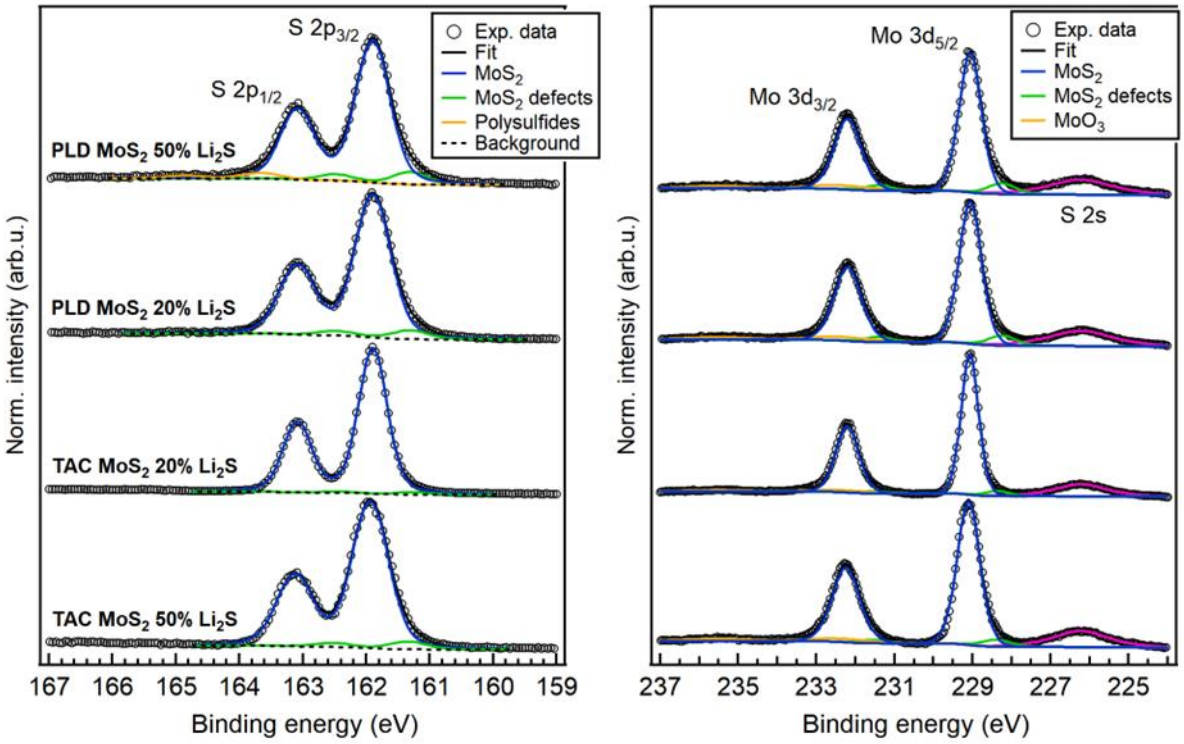

FIG. S3 - S 2p and Mo 3d core level spectra of Li-doped MoS_2 samples taken with hv = 605eV. The main S 2p and Mo 3d components, with S $2p_{3/2}$ at 161.95 eV and Mo $3d_{5/2}$ at 229.05 eV, correspond to thin-film 2H-MoS_2. Small contributions at lower binding energies (S $2p_{3/2}$ at 161.35 eV and Mo $3d_{5/2}$ at 228.3 eV) can be attributed to MoS_2 defect sites, such as sulfur vacancies.[10] Another small contribution to Mo 3d appears at higher binding energies (Mo $3d_{5/2}$ at 232.4 eV), which is attributed to traces of molybdenum oxides formed on the surface due to air exposure.

Tab. TS1 – The chemical composition of pristine and Li-doped PLD and TAC-grown MoS_2 layers. It is worth noting that the PLD samples, even after Li doping, exhibited an S:Mo ratio close to 2.0. Conversely, the S: Mo ratio for TAC-grown MoS_2 layers, both before and after Li-doping, was approximately 2.2. Moreover, TAC-grown samples exhibited traces of impurities, specifically Te, Na, and K. We assume that the contamination originates from the sulfur powder used in their fabrication. Carbon contamination appears relatively high, most likely due to the contribution of the organic species layer formed on the surface upon air exposure and possible graphitic carbon contamination at the substrate or substrate-MoS_2 interface. However, no direct correlation between the carbon contamination level and electron-transport properties was observed.

Sample	Li_2S/S	Equivalent homogenous atomic concentrations (%)						
		Mo	**S**	**Li**	**Te**	**Na**	**K**	**C**
PLD MoS_2[a)]	0%	22 ± 2	45 ± 4	0	n/d	n/d	n/d	33 ± 3
PLD MoS_2	20 %	25 ± 1	52 ± 3	5 ± 3	0	0	0	17 ± 8
PLD MoS_2	50 %	25 ± 1	51 ± 3	7 ± 3	0	0	0	17 ± 8
TAC MoS_2	0%	25 ± 2	56 ± 4	0	0.5 ± 0.2	0.5 ± 0.1	0	17 ± 6
TAC MoS_2	20%	29 ± 1	63 ± 3	4 ± 1	0.3 ± 0.1	0	0	4 ± 1
TAC MoS_2	50%	27 ± 1	60 ± 3	3 ± 1	0.04 ± 0.02	0	0.11 ± 0.02	10 ± 2

[a)] chemical composition analyzed by laboratory XPS.

AFM - Supplementary S4-S5, TS2

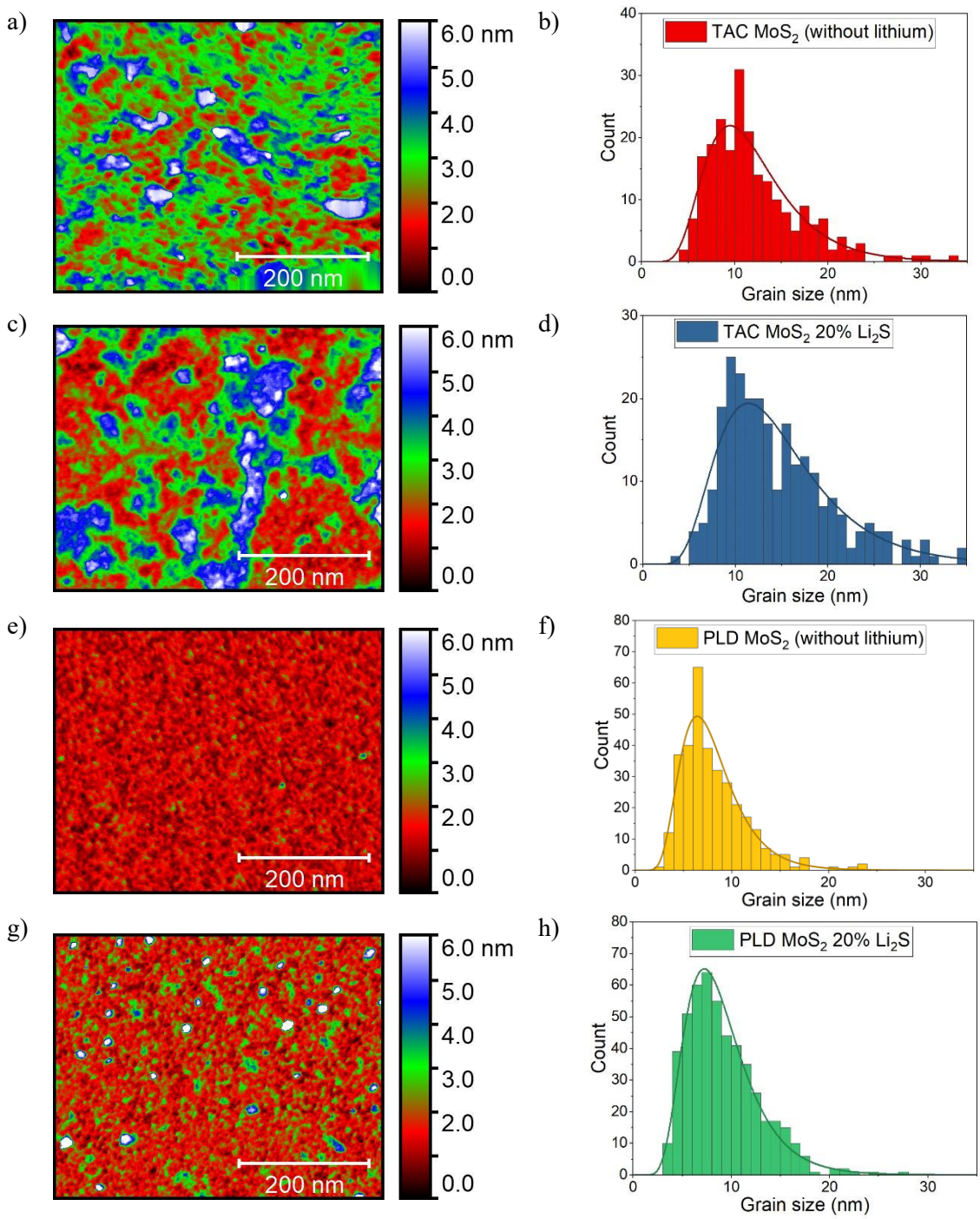

Fig. S4 Atomic force microscopy (AFM) analysis of the MoS_2 layers with and without Li prepared by TAC (a-d) and PLD (e-h). AFM was used to evaluate the surface morphology and topography.
a) AFM scan and b) grain size distribution of undoped TAC-grown MoS_2 layer.
c) AFM scan and d) grain size distribution of Li-doped TAC MoS_2 layer prepared with 20 % of the Li_2S.
e) AFM scan and f) grain size distribution of for undoped PLD-grown MoS_2 layer
g) AFM scan and h) grain size distribution of Li-doped PLD-grown MoS_2 layer prepared with 20 % of the Li_2S.

AFM scans were provided by HR-AFM, Multimode 8 (BrukerNano) with scan areas of 500 x 400 nm with spatial sampling of 1 point per 1 nm. The typical tip radius of fresh AFM was ~ 2 nm to achieve best the resolution of the AFM scan.

The morphology of MoS_2 layers shows a more pronounced height variation for TAC-grown MoS_2 compared to MoS_2 prepared by PLD. For TAC-grown MoS_2 layers, the peak of the grain size distribution is situated around 9 - 10 nm. For PLD-grown samples, the peak of the grain size distribution MoS_2 layers is situated around 6 -7 nm. AFM scans of Li-doped and undoped MoS_2 layers grown by PLD indicate morphology differences after Li-intercalation, while no significant change was observed in the case of TAC samples.

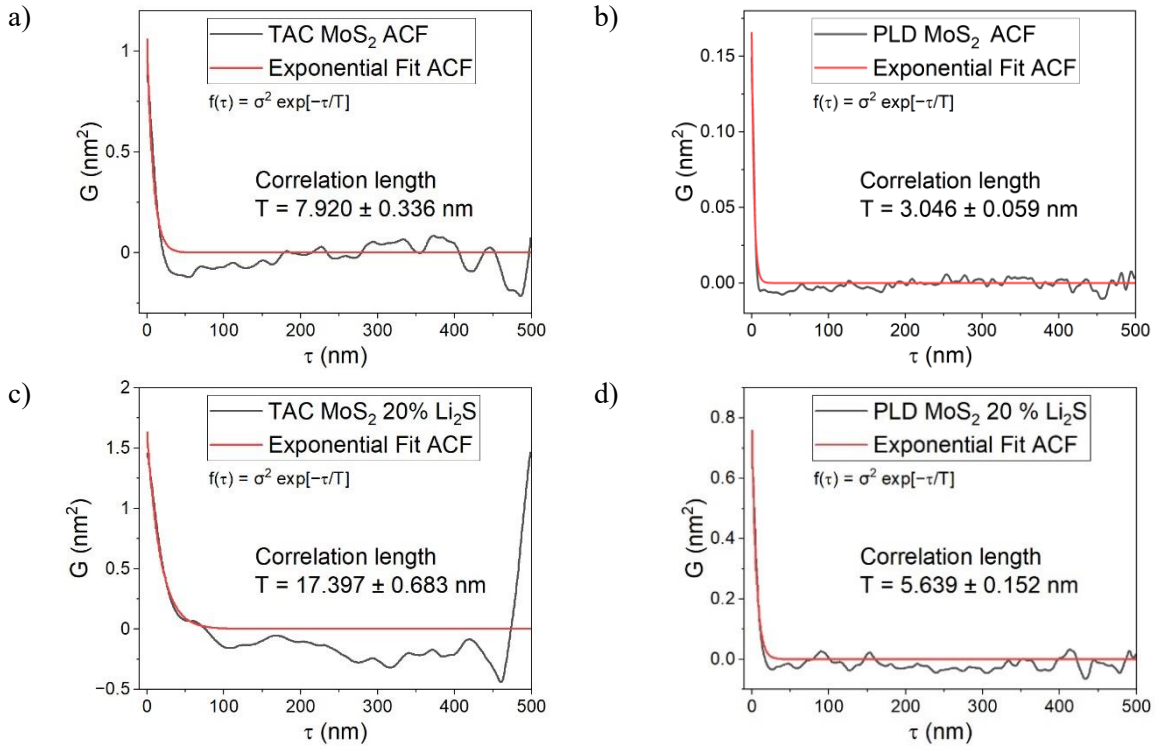

Fig. S5 One-dimensional autocorrelation function (ACF) was performed from the AFM scans of undoped (a) and Li-doped (c) MoS_2 layers grown by TAC and undoped (b) and Li-doped (d) MoS_2 layers grown by PLD. ACF data are approximated by fitting with the exponential function of ACF (the equations are included in Figs), where fitting parameter T represents the correlation lengths of the surface features.

TAB. TS2 Summary of the AFM results.

Sample	RMS Roughness (nm)	Correlation length (nm)	Range of Grain size (nm)
TAC MoS_2	0.941	7.9	4 - 30
TAC MoS_2 20% Li_2S	1.211	17.4	3 - 35
PLD MoS_2	0.387	3.0	2 - 20
PLD MoS_2 20% Li_2S	0.806	5.6	3 - 22

Surface roughness (RMS), Correlation length, and Range of Grain size for Li-doped and undoped MoS_2 layers grown by TAC and PLD are included. The roughness (RMS) of the MoS_2 layer grown by PLD increased from 0.4 to 0.8 nm after Li-intercalation. The roughness (RMS) of TAC samples changes from

0.9 to 1.2 nm after Li-intercalation. Correlation lengths for Li-doped and undoped MoS_2 layers grown by TAC are 17.4 and 7.9 nm, respectively. Li-doped and undoped MoS_2 layers grown by PLD have correlation lengths of 5.6 and 3 nm, respectively. The size of grains for MoS_2 layers grown by TAC and PLD are in the range of 3 - 30 nm suggesting negligible differences of grain sizes for these two fabrication methods. Limits of Correlation length for MoS_2 layers estimated AFM are given by the resolution limits of AFM measurements suggesting that the real correlation lengths could be even smaller than those determined by AFC analysis.

References:

[1] Z. Wang, R. Li, C. Su, and K.P. Loh, "Intercalated phases of transition metal dichalcogenides," SmartMat **1**(1), e1013 (2020).
[2] R. Schlögl, in *Advances in Catalysis* (Elsevier, 2009), pp. 273–338.
[3] L. Wu, N.Y. Dzade, M. Yu, B. Mezari, A.J.F. Van Hoof, H. Friedrich, N.H. De Leeuw, E.J.M. Hensen, and J.P. Hofmann, "Unraveling the Role of Lithium in Enhancing the Hydrogen Evolution Activity of MoS_2: Intercalation versus Adsorption," ACS Energy Lett. **4**(7), 1733–1740 (2019).
[4] N.P. Kondekar, M.G. Boebinger, E.V. Woods, and M.T. McDowell, "In Situ XPS Investigation of Transformations at Crystallographically Oriented MoS_2 Interfaces," ACS Appl. Mater. Interfaces **9**(37), 32394–32404 (2017).
[5] H. Wang, Z. Lu, S. Xu, D. Kong, J.J. Cha, G. Zheng, P.-C. Hsu, K. Yan, D. Bradshaw, F.B. Prinz, and Y. Cui, "Electrochemical tuning of vertically aligned MoS_2 nanofilms and its application in improving hydrogen evolution reaction," Proc. Natl. Acad. Sci. U.S.A. **110**(49), 19701–19706 (2013).
[6] D. Pariari, R.M. Varma, M.N. Nair, P. Zeller, M. Amati, L. Gregoratti, K.K. Nanda, and D.D. Sarma, "On the origin of metallicity and stability of the metastable phase in chemically exfoliated MoS2," Applied Materials Today **19**, 100544 (2020).
[7] G. Drera, G. Salvinelli, J. Åhlund, P.G. Karlsson, B. Wannberg, E. Magnano, S. Nappini, and L. Sangaletti, "Transmission function calibration of an angular resolved analyzer for X-ray photoemission spectroscopy: Theory vs experiment," Journal of Electron Spectroscopy and Related Phenomena **195**, 109–116 (2014).
[8] S. Tanuma, C.J. Powell, and D.R. Penn, "Calculations of electron inelastic mean free paths. V. Data for 14 organic compounds over the 50–2000 eV range," Surface & Interface Analysis **21**(3), 165–176 (1994).
[9] J.J. Yeh, and I. Lindau, "Atomic subshell photoionization cross sections and asymmetry parameters: $1 \leqslant Z \leqslant 103$," Atomic Data and Nuclear Data Tables **32**(1), 1–155 (1985).
[10] M. Donarelli, F. Bisti, F. Perrozzi, and L. Ottaviano, "Tunable sulfur desorption in exfoliated MoS2 by means of thermal annealing in ultra-high vacuum," Chemical Physics Letters **588**, 198–202 (2013).